F. Dehaeze, G. Barakos,
L.I. Garipova, A.N. Kusyumov, A.S. Mikhailov

Coupled CFD/CSD simulation of the helicopter main rotor in high-speed forward flight

Key words: rotorcraft, aeroelasticity, high-speed flight

Abstract

The helicopter main rotor in forward flight is considered in this paper. By comparing results for rigid blades with results for elastic blades, the torsional and flapping blade deformations were extracted from coupled simulations. It was found that a noticeable property of the blade deformation was the strong “dip” in torsional deformation caused by a shock formed on the lower surface on the advancing side of the rotor. The influence of the structural damping coefficient on the blade in-flight deformation isalso considered.

I. Introduction

Rotor CFD/CSD (Computational Fluid Dynamics/Computational Structural Dynamics) calculations are challenging but necessary for accurate simulation results. A coupled CFD/CSD rotor simulation needs to predict the blade deformation due to the flow field, and use it to update and correct the computed aerodynamic forces. In the domestic literature the problem of aeroelastic modeling was mainly solved by eddy methods [1 - 9] in determining the aerodynamic loads to the rotor blades. In Russian references of 70-90 years wind tunnel data for aerofoils used actively at different Mach and Reynolds numbers. It allowed including to consideration influence of flow compressibility. However these approach does not allow modeling of blade tips effects, deformation of the blade shape and transformation of aerofoil shape along the blade span.

An alternative approach to CFD simulation that used in this study is related to solving of the Reynolds-averaged Navier-Stokes equations.

To achieve this, most aeroelastic methods have separate structural and flow solvers that exchange information during computations. Various coupling methods have been put forward in the literature, however, two approaches were mainly used: the weak and the strong coupling. The former consists in an exchange of information between both solvers at every rotor revolution or at every fraction of it, while the latter consists in exchanging information between the two solvers at the end of each time step or even more often. In work [10] compared the strong and weak coupling strategies. While the predictions for the blade deformation were similar, the strong coupling proved more time consuming and less robust. The weak coupling strategy proved more popular, and recently, the interest moved from isolated rotors to full helicopter configurations [12, 13]. Nevertheless, some attempts were also made in using a strong coupling strategy. The main interest of the strong coupling strategy comes from the lack of forced periodicity, which allows the simulation of manoeuvring helicopters, as demonstrated in [13]. Furthermore, other coupling methods including more advanced 3D-FEM structural models were reported in [14, 15], aiming to improve the predictions of the performance of newer rotor blades of advanced planforms.

It has been shown in [16, 17] that for the high-speed flight the torsional deformation played an important role in the rotor load predictions. The torsional deformations determined the hinge moment and were triggered by the movement of a shock on the advancing-side of the rotor, and the formation of a shock on the lower surface of the blade. This case was used in [17], where showed that the inclusion of torsional deformation allowed for improved predictions of the rotor loads on the advancing side, that were mainly driven by a high amplitude pitch-down torsion of the blade near140º of azimuth.

The aim of this work is the aeroelastic analysis of forward flight rotors. Two types of blade deformations were considered for this study: torsional and flapping. The aeroelastic coupling procedure is demonstrated on the UH-60A rotor using the HMB CFD code of the University of Liverpool and the commercial CSD tool NASTRAN for performing modal (frequency) analyses of the rotor blades.

Some other aspects of aeroelastic modeling in 2D aiming at flapped rotor blade sections, were considered in a previous paper [18].

II. Aeroelastic Coupling method

The method developed for HMB first deforms the blade surface using the Constant Volume Tetrahedron (CVT) method, then obtains the updated block vertex positions via the spring analogy method (SAM) and finally generates the full mesh via Transfinite Interpolation (TFI). It is extensively described in [19]. The TFI, first interpolates the block edges and faces from the new vertex position, and then interpolates the full mesh from the outer surfaces of each block. This method uses the properties of multi-block meshes and maintains its efficiency as the number of blocks increases, particularly in the span-wise blade direction.

For forward flying rotors, a modal approach is used. The modal approach allows a reduction of the problem size by modelling the blade shape as the sum of a limited number of dominant eigenmodes, which are obtained using NASTRAN. The blade shape is described as follows:

$$\overline{\varphi} = \overline{\varphi}_0 + \sum \alpha_i \overline{\varphi}_i \tag{1}$$

where vector $\overline{\varphi}$ is the blade shape, $\overline{\varphi}_0$ the blade static deformation, and $\overline{\varphi}_i$ is the *i*-th mass-scaled eigenmode of the blade. The amplitude coefficients α_i are obtained by solving the equations:

$$\frac{\partial^2 \alpha_i}{\partial t^2} + 2\zeta_i \omega_i \frac{\partial \alpha_i}{\partial t} + \omega_i^2 \alpha_i = \overline{f} \cdot \overline{\varphi}_i, \tag{2}$$

where ω_i and ζ_i are respectively the eigenfrequencies and the eigenmode damping ratios, $\overline{f}$ is the vector of external forces. To solve the equation (2) in time, along with the flow solution around the rotor, a strong coupling method was used.

The strong coupling approach does not force periodicity in the blade deformation and may need more time to solve a problem and may also be less stable from weakly-coupled methods. However, it allows more flexibility for complex motions of the helicopter which are not linked to a steady flight (like maneuvers).

Since the HMB method performs time-marching computations using the dual-time step method. One could opt to exchange information between the structural model and the aerodynamic model either at the end of each real-time step or at the end of each Newton sub-iteration. Of course, exchanging information at each Newton step results in more consistent solutions. On the other hand, if the real time-step is small, fewer exchanges between the CFD and CSD methods would also result in correct solutions. Therefore, two approaches were tested and compared in this paper: a leap-frog method (method 1) that computes the modal amplitudes between each real time step, and a strongly implicit method (method 2) which computes the modal amplitudes between each pseudo-time step.

III. Rotor description and modelling conditions

The UH-60A rotor [20] was chosen to assess the aeroelastic coupling strategy. This rotor was tested in flight by NASA and the US Army [21] and in-flight measurements are available for the blade loads. The rotor blade configuration consists of two aerofoil types: SC1095 at the root part of the blade and the SC1094-R8 aerofoil at the middle part of the blade. Besides the tip part of the blade has swept back planform.

The flight conditions and control angles are summarised in Table 1. Table 1 presents parameters: μ is the aspect ratio, M_∞ is the free stream Mach number, Re_∞ is the Reynolds number, a_s is the shaft angle (positive for backward angle), θ_0 is the collective angle, θ_{1c}, θ_{1s} is the cyclic components, β_0 is the coning angle, β_{1c}, β_{1s} is the longitudinal and lateral flapping angles.

The grid contained 8.0 million nodes and the k - ω BSL turbulence model was used. A first simulation was carried out using a structural damping of $\zeta = 0.3$ for every structural mode and an azimuthal step of $\Delta\Psi = 0.25^o$ was used (the rotor rotates in the anti-clockwise direction). The first half of the revolution was run as a rigid case, before the blade was allowed to elastically deform. Three revolutions allowed for convergence of the deformations and loads.

Table 1. UH-60A flight conditions and trimming for flight counter 8534 (the angles

are given in degrees)

μ	M_∞	Re_∞	a_s	θ_o	θ_{1c}	θ_{1s}	$ß_o$	$ß_{1c}$	$ß_{1s}$
0.368	0.256	2.735 ×	-7.31	11.6	-2.39	8.63	3.43	-0.70	-1.00

The blade structural properties were estimated from information available in the literature [20], however, some uncertainties still exist on the exact blade geometry, twist distribution and structural model.

IV. Results from aeroelastic computations

The blade deformations were extracted from the coupled simulations and are shown in Figure 1. The most noticeable property of the blade deformation is the strong dip in torsional deformation at the advancing side. This deformation is caused by a shock formed on the lower surface of the blade as shown in Figure 2. The blade recovers from the torsional deformation when the local free stream velocity decreases enough for the strength of the shock to lower. The amplitude of the second torsional mode seemed negligible compared to the amplitude of the first torsional mode. The flapping deformation also seemed to be dominated by the second flapping mode, with a strong dip of the blade tip at $\Psi = 135°$.

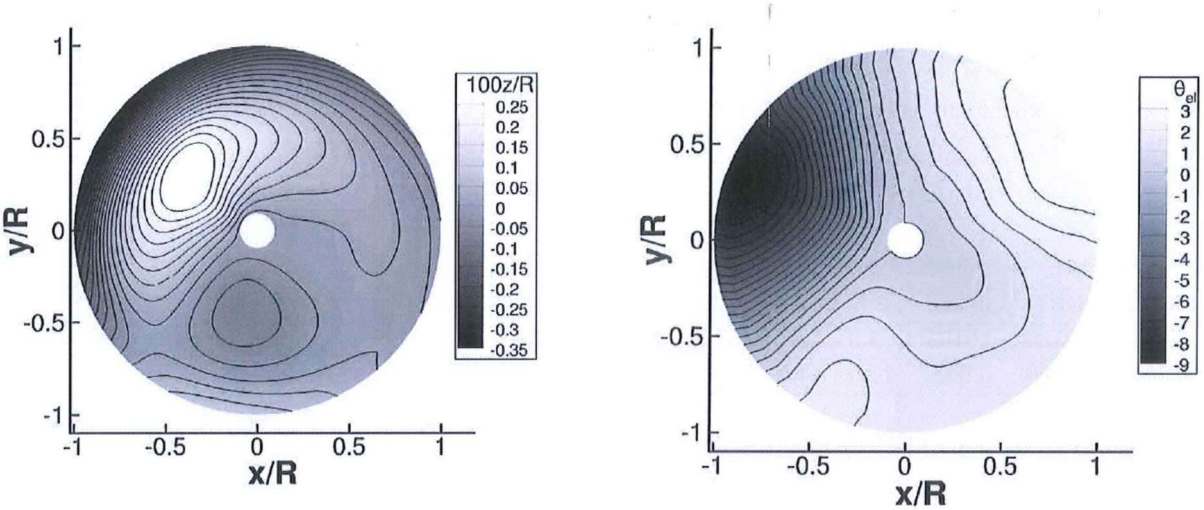

a) b)

Figure 1. Predicted UH-60A blade deformation during a revolution:

a) Elastic flapping; b) Elastic torsion

The Mach-scaled sectional normal force and pitching moments were

extracted and are shown in Figure 3. The influence of the torsional deformation around Ψ = 160° is clearly visible, with a negative normal force.

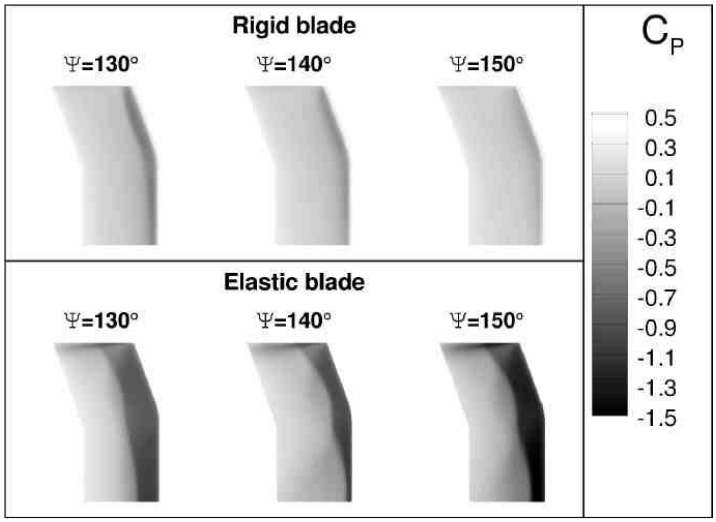

Figure 2. Comparison of the pressure coefficient on the blade lower surface between a rigid blade assumption and an elastic blade

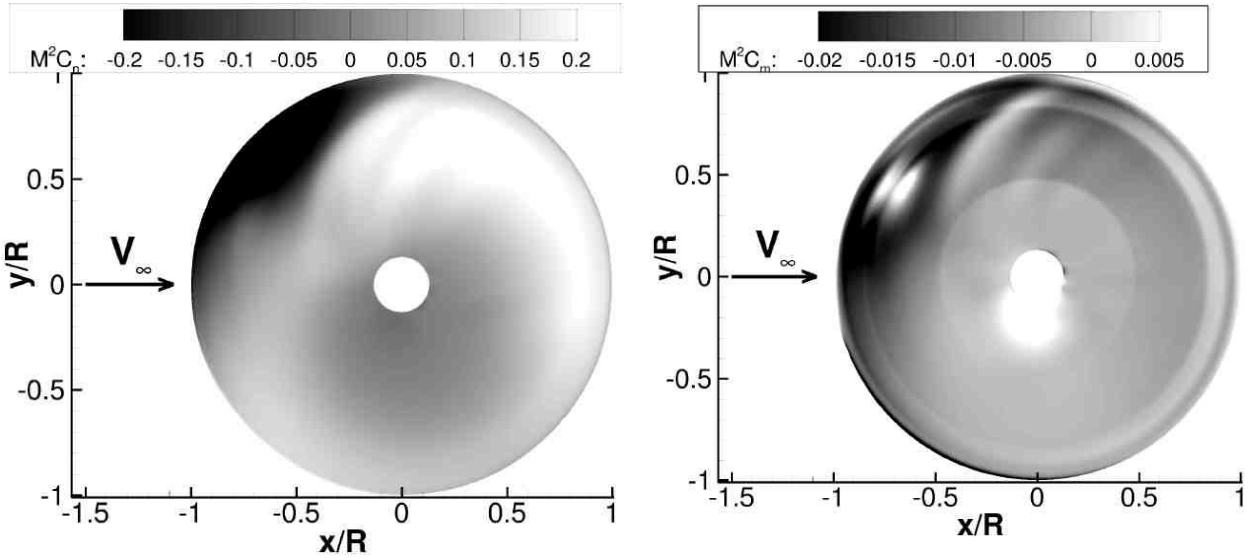

(a) *(b) M^2Cm*

Figure 3. Scaled loading of the UH-60A: a) normal force M^2C_n; b) pitching moment M^2C_m

The sectional normal force is compared with flight-test measurements [21] at two radial positions (r/R=0.675 and r/R=0.865) in Figure 4. The dip in the sectional forces on the advancing side appeared stronger in the simulations than in the flight test measurements, and was delayed by 15°. However, the loads on the retreating side agreed better with the flight test measurements. At r/R = 0.675, the

BVI predicted by the simulations did not seem to occur in the flight tests on the advancing-side, but at r/R = 0.865, their locations and amplitudes seem to agree with the flight test data. The mean normal force in the first quadrant is, however, over-predicted.

The predicted loads were also compared to the ones obtained with a rigid blade (Figure 4) and the ones obtained in [17], using a prescribed torsion closer to the flight tests data.

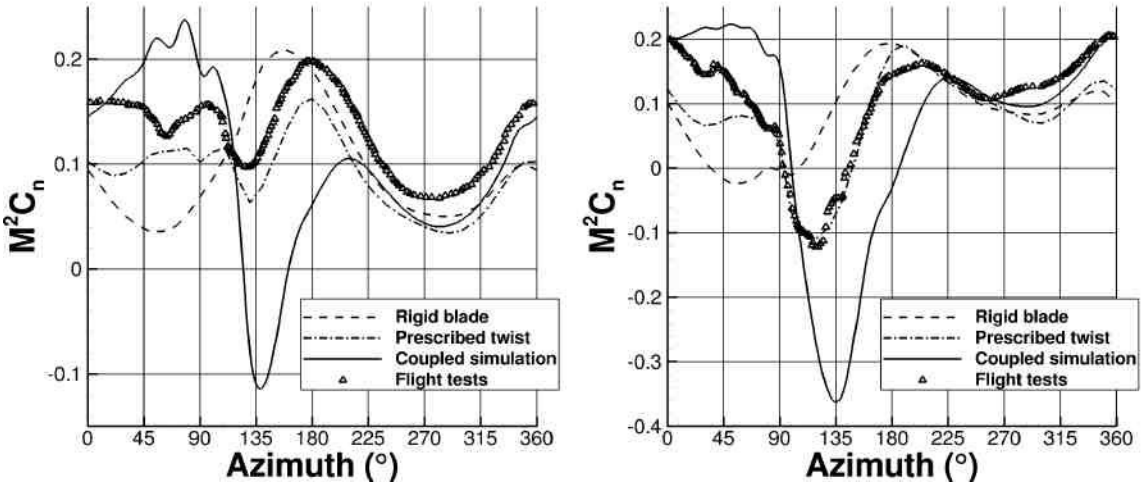

a) b)

Figure 4. Comparison of the sectional normal force of the UH-60A with flight test measurements for Flight 8534: a) r/R = 0.675; б) r/R = 0.865

On the advancing side and towards the front of the rotor disk, high frequency oscillations can also be noticed. These are caused by Blade Vortex Interaction (BVI). Looking at the pitching moments, the transition between aerofoil sections and the start of the sweep can be noticed through the moment discontinuities in the radial direction. The higher moments due to the SC1094-R8 aerofoil seemed to trigger the dip in the torsional moment, due to the higher amplitude of the pitching moment between $\Psi = 45°$ and $\Psi = 120°$.

The BVI around $\Psi = 85°$ also appeared to be stronger in the coupled simulation compared to the others, which comes from the inclusion of the flapping deformation. Clearly, the approximate blade shape and the lack of detailed data for the structural properties have an influence on the results.

It was then decided to study the influence of the structural damping coefficient ζ (see Equation 1) on the blade deformation. Therefore, damping coefficients of $\zeta = 0.02$ and $\zeta = 0.1$ were compared to the original value of 0.3. The evolution of the blade tip deformation with the damping coefficient can be seen in Figure 5. The main features of the blade deformation did not change. The tip flapping showed a difference in the recovery from the dip on the advancing side. With the lower damping, the recovery happened at a higher speed, and the overshoot was also more pronounced. Also, the aerodynamic damping on the retreating side proved low, and a decrease in the structural damping allowed the blade to vibrate at the frequency of the first torsional mode.

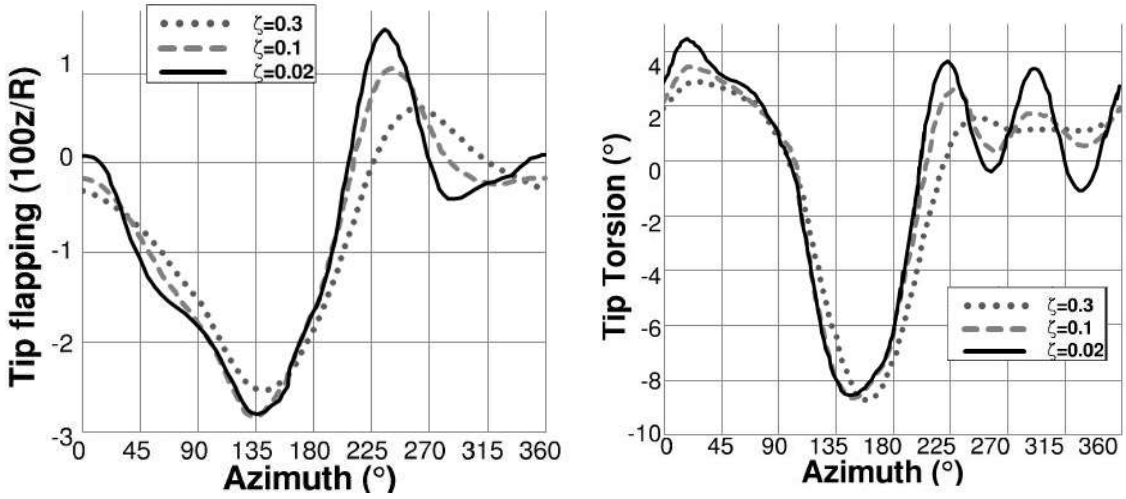

a) b)

Figure 5. Predicted blade tip deformations for several structural damping coefficients: a) Tip flapping; b) Tip torsion

The influence of the azimuthal time step was also studied, using $\Delta\Psi = 1°$ and $\Delta\Psi = 0.25°$. The strongly implicit method (method 2) was used for these computations. The obtained tip deformations are shown in Figure 6. The difference in the blade deformation predictions was limited to the advancing side and to the tip torsion, with an earlier recovery from the dip when using $\Delta\Psi = 0.25°$.

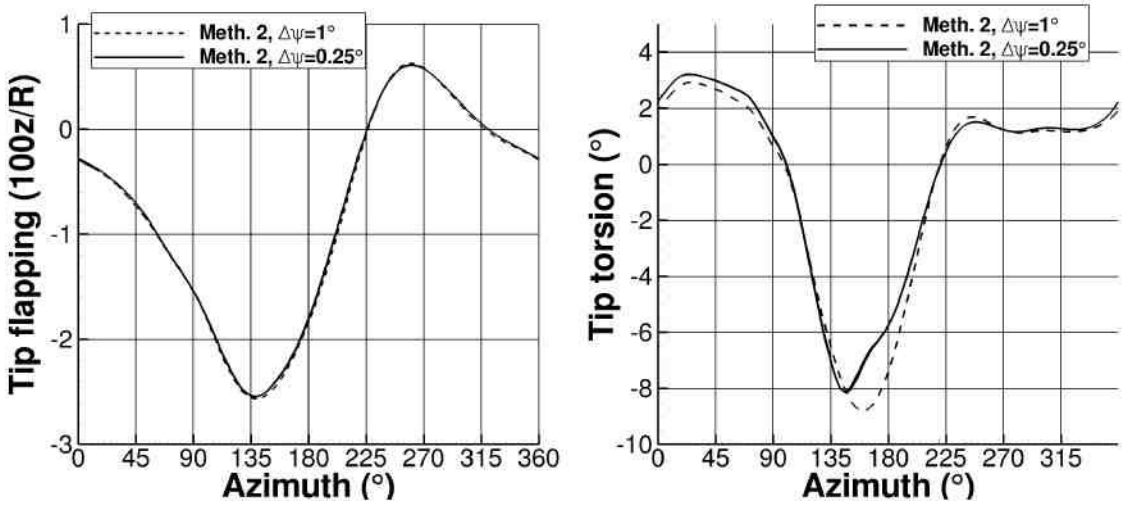

a) b)

Figure 6. Effect of the time step on the predicted blade tip deformations: a) Tip flapping; b) Tip torsion

Therefore, a time step $\Delta\Psi = 0.25°$ was used to compare the two proposed coupling methods: the leap-frog (method 1) and the implicit method (method 2). Figure 7 shows the tip deformation for the two methods: the difference between the two methods proved limited.

Finally, the influence of the turbulence model was assessed, with the use of the k - ω BSL and SST turbulence models [22]. A time step of $\Delta\Psi = 0.25°$, and damping ratio of $\zeta = 0.3$ were used. The tip deformation predictions are shown in Figure 8. The main difference was located on the dip: a 0.7 degrees difference was visible in the dip of the tip torsion. This difference is due to the small differences in strength of the shock appearing on the blade tip area.

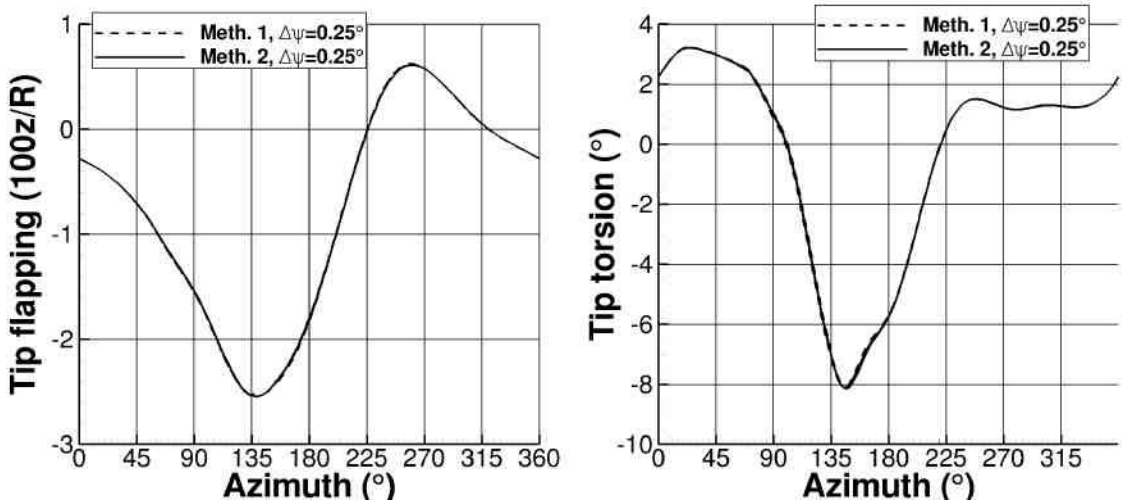

a) b)

Figure 7. Comparison of the predicted blade tip deformations with for two coupling methods (1 is the leap-frog method and 2 is the implicit coupling method): a) Tip flapping; b) Tip torsion

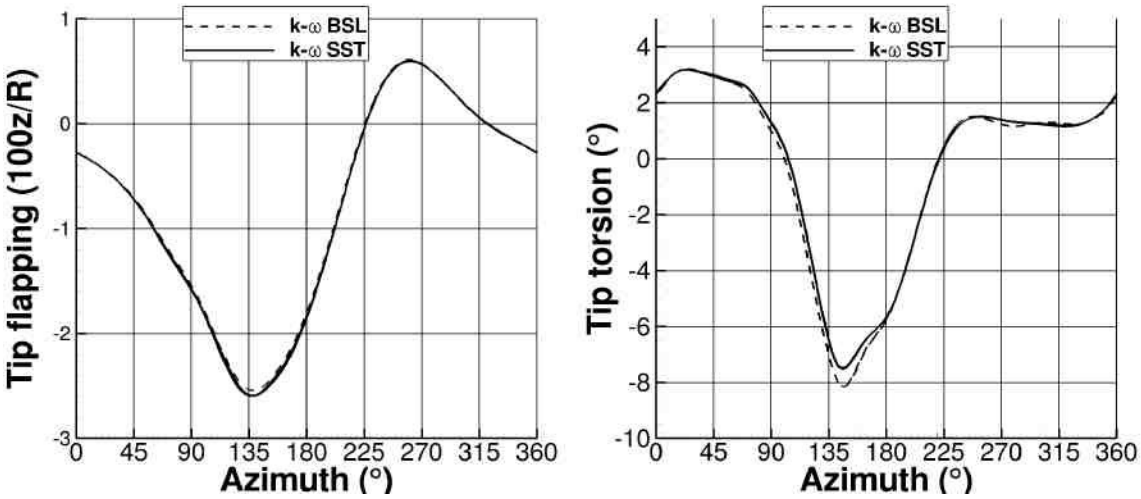

a) b)

Figure 8. Influence of the turbulence model on the predicted UH-60A blade tip deformation: a) Tip flapping; b) Tip torsion

V. Summary and Conclusions

A strongly coupled CFD/CSD method was applied to the UH-60A rotor in high-speed forward flight. The method proved to be able to predict the strong torsion peak on the advancing side of the rotor that was also present in the flight tests. The leap-frog coupling method was also used and it was found that it also provided adequate results although the strong coupling was slightly better. The influences of the structural damping coefficient, the employed time step of the simulations, and the turbulence model on the obtained results were also investigated.

The support of this work via the"State tasks in the field of scientific activity" (No 9.1694.2014/K) grant is gratefully acknowledged.

References

1. Belotserkovsky S.M., Loktev B. E., Nisht M.I. Research on the computer the aerodynamic and aeroelastic characteristics of helicopter rotor. - Moscow: Engineering, 1992, pp 88-100 [in Russian].

2. Mikhailov S.A., Nikolaev E.I., Garipov S.A. Derivation of equations of oscillations rotor blades with taking into account the spatial movement of the helicopter // Russian Aeronautics (Iz VUZ). № 2. – 2005, pp. 3-7 [in Russian].

3. Grishanina T.V., Kvak Je Hwang. Application of the finite element method to the calculation of non-linear oscillations of a rotating blade // Bulletin of the Moscow Aviation Institute, 2009. T. 16. No 5, pp 296-299 [in Russian].

4. Mil M.L. and others. Helicopters. Calculation and design. Vol 1. Aerodynamics / Mil M.L., Nekrasov A.V., Braverman A.S., Grodko L.N., Leykand M.A. // Moscow: Engineering, 1966. - 456 p. [in Russian]

5. Golovkin A.V., Kalyavkin V.M. Some features of blade loading of a high load main rotor // Main rotor qerodynamics (digest). – TsAGI Transactions, 1975, relise. 1685, pp. 75-81. [in Russian]

6. Liss A.Yu. Calculation of the air rotor blades in flight // Aviatsionnaya technica. 1973. -№ 2, pp. 40-45. [in Russian]

7. Anikin V.A. Some results of the “vortex ring” mode for a coaxial rotors / Anikin V.A., Loktev B.E., Simonenko V.A.// Scientific and methodical materials on the aerodynamics of the aircraft. Nonlinear characteristics. Moscow: VVIAIM named after Prof. N.E. Zhukovsky, 1982, pp. 257 – 266. [in Russian]

8. Leontiev V.A. The method of solving of the elastic blade helicopter rotors motion equations in general movement//TsAGI Scientific Notes. № 5, Vol. XLI, 2010, pp. 67 – 80. [in Russian]

9. Burtsev B.N. Features of the stress-strain state of the rotor blades root part/ Burtsev B.N., Tyutyunnikov H.P.// Mekhanika Kompozitsionnykh Materialov i Konstruktsii. - 2012. -Vol. 18, № 4, pp. 552-561. [in Russian]

10. Altmikus A., Wagner S., Beaumier P., and Servera G. A Comparison: Weak versus Strong Modular Coupling for Trimmed Aeroelastic Rotor

Simulations // American Helicopter Society 58th Annual Forum, June 2002.

11. Dietz M., Kessler M., and Kràmer E. Trimmed Simulation of a Complete Helicopter Configuration Using Fluid-Structure Coupling // High Performance Computing in Science and Engineering ‘07, Springer Berlin Heidelberg, 2008, pp. 487–501.

12. Biedron R. and Lee-Rausch E. Computation of UH-60A Airloads Using CFD/CSD Coupling On Unstructured Meshes // American Helicopter Society 67th Annual Forum, Virginia Beach, VA, May 3–5 2011.

13. Sitaraman J. and Roget B. Prediction of Helicopter Maneuver Loads Using a Fluid-Structure Analysis // Journal of Aircraft, Vol. 46, No. 6, November–December 2009, pp. 1957–1964.

14. Ortun B. Petot D. Truong K. and Ohayon R. Towards a New Generation of Rotorcraft Comprehensive Analysis; Coupling with CSM and CFD // 34th European Rotorcraft Forum, Liverpool, UK, September 16–18 2008, Paper 6a2.

15. Datta A. and Johnson W. A Multibody Formulation for Three Dimensional Bick Finite Element Based Parallel and Scalable Rotor Dynamic Analysis // American Helicopter Society 66th Annual Forum, Phoenix, AZ, May 11–13 2010.

16. Datta A., Sitaraman J., Chopra I., and Baeder J. CFD/CSD Prediction of Rotor Vibratory Loads in High-Speed Flight // Journal of Aircraft, Vol. 43, No. 6, November–December 2006, pp. 1698–1709.

17. Steijl R., Barakos G., and Badcock K. Computational Study of the Advancing-Side Lift-Phase Problem // Journal of Aircraft, Vol. 45, No. 1, January–February 2008, pp. 246–257.

18. Steijl R. Dehaeze F. Barakos G.N. Garipova L.I. Kusyumov A.N. and Mikhailov A.S. Simulation of flow around a blade section with one degree of freedom aeroelastic flap // Russian aeronautics (Iz.VUZ), 2015, № 2. P. 54-59.

19. Dehaeze F. and Barakos G. Mesh Deformation Method for Rotor Flows // Journal of Aircraft , Vol. 49, No. 1, January–February 2012, pp. 82–92.

20. Arcidiacono P. and Zincone R. Titanium UTTAS Main Rotor Blade //

Journal of the American Helicopter Society, Vol. 21, No. 2, 1976, pp. 12–19.

21. Leung J., Wei M., and Aoyagi M. UH-60A Airloads Data Acquisition and Processing System // AIAA/IEEE 13th Digital Avionics Systems Conference, October 30 November 3 1994, pp. 206–211.

22. Menter F. Two-Equation Eddy-Viscosity Turbulence Models for Engineering Applications // AIAA Journal, Vol. 32, No. 8, 1994, pp. 1598–1605.